Applied Soft Computing 52 (2017) 348–358

Contents lists available at ScienceDirect

Applied Soft Computing

journal homepage: www.elsevier.com/locate/asoc

Automatic surface defect detection for mobile phone screen glass based on machine vision

Chuanxia Jian*, Jian Gao, Yinhui Ao

Key Laboratory of Mechanical Equipment Manufacturing & Control Technology of Ministry of Education, School of Electromechanical Engineering, Guangdong University of Technology, Guangzhou 510006, Guangdong, PR China

ARTICLE INFO

Article history:
Received 1 March 2016
Received in revised form 8 September 2016
Accepted 24 October 2016
Available online 25 October 2016

Keywords:
Mobile phone screen glass
Defect detection
Contour-based registration
Image subtraction
Fuzzy c-means cluster

ABSTRACT

Defect detection using machine vision technology plays an important role in the manufacturing process of mobile phone screen glass (MPSG). This study proposes an improved detection algorithm for MPSG defect recognition and segmentation. Considering the problem of MPSG image misalignment caused by vibrations in the mobile stages, a contour-based registration (CR) method is used to generate the template image used to align the MPSG images. Based on this registration result, the combination of subtraction and projection (CSP) is used to identify defects on the MPSG image, which can eliminate the influence of fluctuation in ambient illumination. To segment the defects with a fuzzy grey boundary from a noisy MPSG image, an improved fuzzy c-means cluster (IFCM) algorithm is developed in this study. A defect detection system is developed, and the proposed algorithms are validated using a number of experimental tests on MPSG images. The testing results demonstrate that the approach proposed in this study can effectively detect various defects on MPSG and that it has better performance than other methods.

1. Introduction

The quality of mobile phone screen glass (MPSG) is an important consideration during the manufacturing process of mobile phones. MPSG with common surface defects, such as scratches, chips and dirt, should be identified and removed during manufacturing in real time. Four types of common defects that occur in the manufacturing process are scratches, chips, dirt and light leaks, as shown in Fig. 1.The corresponding causes for these defects are listed in Table 1. The sizes of MPSG surface defects are significantly smaller (*e.g.*, approximately 0.05 mm), which complicates their defect detection. Additionally, the printed section of the MPSG surface makes it more difficult to find and segment a defect.

Currently, recognizing these defects primarily depends on human eye inspection and requires approximately 15 s of a worker's time to fully inspect a single MPSG surface for defects. Defect detection based on machine vision has already been widely implemented in industry [1–4]. Liang et al. [5] proposed a sparse representation in low resolution image to efficiently and quickly detect the surface defects of mobile phone cover glass. Li et al. [6] proposed the principle components analysis to find and extract the defects of touch screen glass. Torng et al. [7] developed a multi-function automated optical inspection system for the mobile phone panels in the production line, and the system can detect both the 2D defects on the whole panel and the uniformity of 3D film thickness of the glass coating. However, these approaches are sensitive to the surrounding illumination variation. Approaches to defect detection are broadly divided into the following three categories.

(1) Classification. Defect detection can be considered as binary classification of normal and abnormal. In this line, feature extraction and classification are two critical steps [8,9]. Mitra et al. [10] presented a neural network architecture using a support vector machine as an inference engine for classification of light detection. Liu et al. [11] studied the surface defects of TFT-LCD manufacturing process, and proposed automatic inline defect detection using grey features and support vector data description. Zhang et al. [12] selected features of Windows Registry access recorder, and implemented the standard SVM, weighted SVM and one class SVM for defect detection.
(2) Background reconstruction and removal (BRR). The methods reconstruct and remove repetitive or texture background image, then find defects in the residual image. The primary task is how to reconstruct background image. Tsai et al. [13] constructed a 3D image, used band-rejecting filtering to eliminate the inhomogeneous textures of sputtered glass, and back-

* Corresponding author.
E-mail address: jianchuanxia@163.com (C. Jian).

http://dx.doi.org/10.1016/j.asoc.2016.10.030
1568-4946/

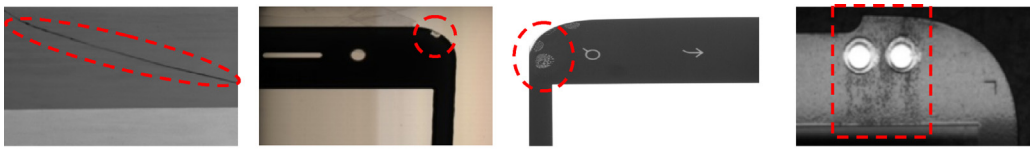

Fig. 1. Common defects in MPSG.

Fig. 2. The MPSG image.

Table 1
Typical defects in MPSG and the corresponding possible causes.

Common defects	Cause of occurrence
Scratch	Misused equipment
Chip	Uneven force on the glass edge during the initial cutting, notch and edge grinding.
Dirt	Ink is misprinted on the non-ink area of the glass, or other particles attach to the glass.
Light leak	Light can pass through the printing area of the glass due to uneven ink thickness.

transformed the data to reconstruct the image; the residual image distinctly preserved the defects. Jung et al. [14] used the Fourier spectrum to eliminate the periodic cell pattern of a TFT-LCD for defect detection. Lu and Tsai [15] proposed using the singular value decomposition to eliminate the repetitive horizontal and vertical elements of a LCD to preserve the defects in the residual image.

(3) Template reference. Defects can often be found through comparing a template image with a test image [16–18]. Xie and Guan [19] presented a novel golden-template self-generating technique for detecting possible defects in periodic two-dimensional wafer images, and the golden template was obtained from the wafer image itself without any prior knowledge. Chou et al. [20] described an automated defect classification system of semiconductor chips at various manufacturing steps, which used a golden template method for defect detection.

Besides these approaches, some other approaches were also investigated [21,22]. In the following, we try to compare the three-category approaches in MPSG surface defect detection. For the classification methods, the speed and accuracy of defect detection were often degraded by undistinguished feature, feature data of higher dimensionality and classifier of weak generalization performance [23–26]. If the methods were used to detect the MPSG surface defects, we need to carefully address feature selection, feature dimensionality reduction and classifier generalization performance improvement. Any omission may cause high false defect detection. The BRR approaches attempted to detect the surface defects of industrial products (such as TFT-LCDs, solar modules and sputtered glass) whose image backgrounds contained either periodic/self-similar patterns or statistical texture structures. However, these patterns or structures are significantly different from the surface structure of MPSG where there is a printed region (the white region) and a non-printed region (inside the white region), as shown in Fig. 2. Therefore the BRR approaches can not effectively find possible defects in MPSG image. Template reference is a well-known and effective approach for defect detection in the industry [16–18,27,28]. This approach is very fast because it is only involved in arithmetical operation of pixels, thereby it can meet the high demand of online detection. Thus, the approach is initially used for defect detection process with a MPSG surface in this study.

In the template reference methods, several critical problems need to be considered: misalignment, surrounding illumination variations and fuzzy boundary defect segmentation. Contour-based registration (CR), the combination of image subtraction and greyscale projection (CSP), and the improved fuzzy c-means cluster (IFCM) are proposed to solve these problems in this study paper. The remainder of this paper is organized as follows. Each of these problems is discussed in detail, and the corresponding solutions are identified in section 2. The defect detection system for MPSG is formulated in Section 3; CR, CSP and IFCM are also presented in detail. In Section 4, the performances of CR, CSP and IFCM are determined using experimental results. Section 5 presents the conclusions and identifies areas for future work.

2. Problem description and solutions

2.1. Misalignment

The captured MPSG images may slightly displace and rotate due to vibrations in the stage. If the captured images were not aligned pixel-by-pixel to the template, significant errors would result during image subtraction. Meanwhile, the average of multiple free-defect images was used to create the template [29,30], and misalignment of these free-defect images would produce an inaccurate template. The primary task thereby is alignment. The methods of image registration can be divided into two parts: the grey-based methods and the feature-based methods [31]. The grey-based methods carry out image registration using the greyscale values of all pixels, therefore the speed is slow, especially for the MPSG image of large size 2500×2000. Additionally, they are very sensitive to illumination variations [32]. The feature-based methods can solve the problems caused by the grey-based methods [33]. Contour is one of common features used for alignment. In the case of rotation and translation, the contour geometry remains unchanged. Thereby contour-based registration (CR), in this study, was proposed to take advantage of contour features (*i.e.*, touch keys and earpieces) present on the MPSG specimens.

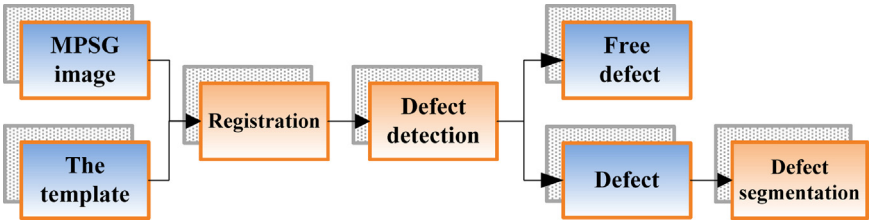

Fig. 3. Flowchart of the proposed automatic MPSG surface defect detection system.

2.2. Test images grey fluctuation from illumination variations

Image subtraction between the template $g(x, y)$and the test image$f(x, y)$ is used to obtain the residual image$R(x, y)$:

$$R(x, y) = |g(x, y) - f(x, y)| \quad (1)$$

The grey levels of the test image change with illumination variations, which leads to greyscale fluctuation in the residual image; thus, finding defects using image subtraction is not reliable. To weaken the affection of illumination variations, Wang and Yung found objects from the test image using multiple adaptive thresholds and boundary evaluation [34]. Liao et al. proposed scale invariant local patterns to handle the illumination variations [35]. Gaussian mixture modelling (GMM) was well known to be effective to address illumination variations [36,37]. However these methods still suffer from a high false alarm because of over-quick and arbitrary illumination variations. Wang et al. proposed using greyscale projection for surface defect detection on steel strips; this method was independent of the surrounding illumination levels [38]. However, this technology used the homogeneous grey background of the steel strips, which is significantly different from the MPSG surface. This condition can be mimicked on MPSG using the following process. After aligning the test image and the template, we can eliminate the printed region using image subtraction to obtain a homogeneous grey texture in the residual image. We then find the presence or absence of defects using greyscale projection. The proposed method combines the results of image subtraction and greyscale projection.

2.3. Fuzzy boundary defect

Some defects are located near the background in the grey level distribution, which prevents their boundary from being clearly defined by human eyes. It is difficult to effectively determine the boundary pixels using common threshold segmentation techniques. Hashioka et al. [39] proposed fuzzy object shape model for fuzzy boundary newborn brain MR image segmentation. Bi et al. [40] proposed using level set method for accurately segmenting fuzzy boundary defect. In this study, a new region-based active contours model was used for more suitable to segmentation of fuzzy boundary Mura defects. Based on this new model, the level set method accurately segmented Mura defects. However, how to choose the parameters of model was still not a standard of theoretical knowledge as a guide. Based on the inaccuracies present in the boundary pixels, we assign pixels to the initial membership function$A(x)$and identify boundary pixels based on the final$A(x)$after multiple iterations. Fuzzy c-means clustering (FCM) can accurately classify fuzzy pixels using$A(x)$; however, FCM is sensitive to noise because it doesn't consider the space relationship between the pixels [41–43] and is thus not suitable for defect segmentation in a noisy MPSG image. Therefore, we propose using an improved FCM (IFCM) to solve this problem.

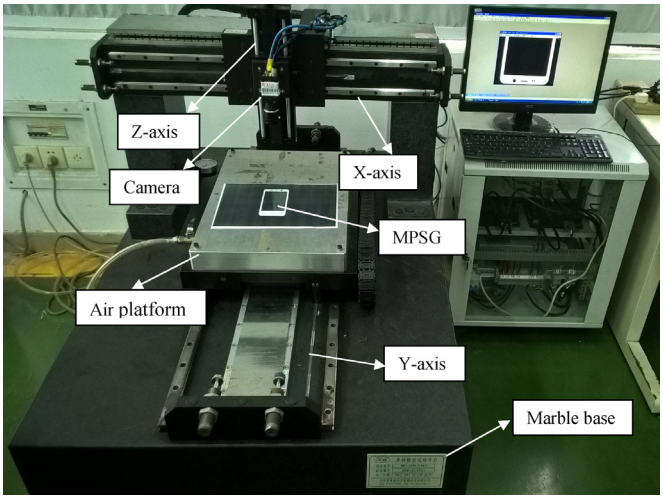

Fig. 4. Experimental stage for capturing the MPSG.

3. Automatic defect detection system for MPSG

The proposed automatic defect detection system for MPSG consists of three stages: registration, defect detection and segmentation. In the first stage, multiple defect-free MPSG images are aligned to generate a template; then, the test image is aligned with the template for defect detection. In the second stage, the template is subtracted from the test image to produce a residual image. The greyscale projection of the residual image is then used to determine the presence or absence of defects. If defects are present, the MPSG is removed from the manufacturing process, and the corresponding data are sent to the next stage for defect segmentation. In the third stage, an improved FCM method is used for accurate defect segmentation. The flowchart of the proposed automatic MPSG surface defect detection system is shown in Fig. 3.

3.1. Image acquisition

The size of the MPSG used in this study is 130 mm by 65 mm and requires a high visual detection accuracy of 0.05 mm to identify small defects. In the experiment, we used the monochrome camera FC5200GE (manufactured by the Japan TAKENAKA system CO., LTD) with a CCD resolution of 2500×2000 pixels. Fig. 4 shows the experimental platform system of the image acquisition process. The platform system was manufactured by the Beijing SmartMotion Electronic Systems Technology Co., Ltd. The location accuracy of the platform system is 1 μm, and the maximum acceleration is 2 g. The size of the platform system is 1200 × 850 × 800 mm. The maximum travels of the X-axis direction (*i.e.*, horizontal) and the Y-axis direction (*i.e.*, fore and aft) are both 500 mm. The MPSG is fixed on a mobile stage and moves along the Y-axis of the mobile stage. The CCD camera moves with the lead screw head in the X-axis direction to ensure that the reflected light from the MPSG surface reaches the camera; the camera also moves with the head in the Z-axis direction (*i.e.*, vertical) to ensure that the right working

distance is maintained. Half of the MPSG image in the experiment is captured to ensure image quality. The captured image is an 8-bit grey-level image of size 2500 × 2000 in BMP format. The size of a pixel in the image is approximately 0.0325 mm (*i.e.*, 65 mm/2000pixels = 0.0325 mm/pixel).

3.2. Proposed contour-based image registration

In the experiment, the CCD camera cannot hold the whole MPSG. Half of the MPSG image is captured for each timeframe. The other half is obtained in the next capture. One of the two images contains the patterns (*i.e.*, touch keys and earpieces), and we implement the registration for the image containing the patterns. The registration results are applied to the other half of the MPSG image because the two half images of a MPSG have the same geometric transform.

The half of the MPSG image with the patterns is firstly cropped to a region which probably contains patterns to implement image registration. Then, noise is removed using the open operation in the morphology, and the region's binary image is obtained using the Otsu method. Finally, pattern contours can be extracted from the binary image using edge detection operators. Since the invariant moment only depends on the geometry of the object, it remains constant in the case of the object's displacement and rotation. Therefore, Hu's invariant moments $\phi_i (i = 1, 2, \cdots 7)$, in this study, are introduced to describe the pattern features in the MPSG image [44]. A similarity measure(*SM*) for image registration is defined as follows based on Hu's invariant moments:

$$SM = \sum_{i=1}^{7} \left| \frac{\phi_i - \hat{\phi}_i}{\phi_i + \hat{\phi}_i} \right| \tag{2}$$

where ϕ_i and $\hat{\phi}_i$ are Hu's invariant moments of the corresponding contours. When the geometries of the contours are similar, $\phi_i$is near$\hat{\phi}_i$ and *SM*approaches zero; the corresponding contours of the smallest *SM* can thus be aligned. The transformation parameters can be evaluated by:

$$\begin{pmatrix} \hat{x} \\ \hat{y} \end{pmatrix} = \begin{pmatrix} \cos\theta & \sin\theta \\ -\sin\theta & \cos\theta \end{pmatrix} \begin{pmatrix} \bar{x} \\ \bar{y} \end{pmatrix} + \begin{pmatrix} \Delta x \\ \Delta y \end{pmatrix} \tag{3}$$

where$(\bar{x}, \bar{y})$and$(\hat{x}, \hat{y})$ are the corresponding centroids of the aligned contours; θ is the angle of the rotation; andΔx and $\Delta y$are the differences between the two centroids along the X-axis and Y-axis, respectively.

3.3. Proposed CSP method for defect detection

As stated previously, greyscale projection of the residual image is used to identify the presence or absence of a defect. Using the $m \times n$ image$f(i, j)$, the pseudocode of the greyscale projection algorithm is described as follows:

Algorithm 1.

1: **for** $i = 1 \text{ to } m$

2: $R(i) = sum(f(i,:)/n)$;

3: **end for**; % Calculate the average grey of all pixels in every row.

4: **for** $j = 1 \text{ to } n$

5: $C(j) = sum(f(:, j)/m)$;

6: **end for**; %Calculate the average grey of all pixels in every column.

7: $C = \max(C(j)) - \min(C(j))$;

8: $R = \max(R(i)) - \min(R(i))$;

9: $T = \max(C, R)$;

10: **if** $T < T_{threshold}$ **then** % $T_{threshold}$ is set at the beginning.

11: output no defects;

12: **else if** $T \geq T_{threshold}$ **then**

13: output defects;

14: end if

$T_{threshold}$can be set by evaluating the greyscale distribution of multiple defect-free images in the experiments. In this study,$T_{threshold}$is set to be 16. C can be obtained when the minimum is subtracted from the maximum for all columns of the greyscale averages. When the surrounding illumination changes, Cremains constant because the maximum illumination has the same amount of fluctuation as the minimum, which can be clearly expressed in Eq. (4).

$$C = [\max(C(j)) + \lambda] - [\min(C(j)) + \lambda] = \max(C(j)) - \min(C(j)) \quad (4)$$

whereλ is the amount of greyscale fluctuation due to illumination variations. The value ofλ might change with the illumination change and the CCD response; however, the λ change cannot affect the value of Cbecause the fluctuation level of λ is the same for $\max(C(j))$ and $\min(C(j))$. The parameter λ is eliminated from the subtraction operation, as shown in Eq. (4).

3.4. Proposed IFCM method for defect segmentation

The FCM method was first proposed by Dunn [45]. In his studies, he attempted to locate $c$clusters by partitioning all of the pixels in an image based on each pixel's grey level; this method assigned the initial membership function to each pixel randomly. Then, the final membership and clustering centre could be obtained after the iterations by minimizing the objective function, which is defined as follows:

$$\begin{aligned} &min \;\; J_m(U,V) = \sum_{i=1}^{c}\sum_{k=1}^{n} u_{ik}^m \|x_k - v_i\|^2 \\ &s.t. \;\; \sum_{i=1}^{c} u_{ik} = 1, \quad i \in [1,c], \quad k \in [1,n], \quad u_{ik} > 0 \end{aligned} \quad (5)$$

where $U = [u_{ik}]$ is the membership matrix;$u_{ik}$is the membership of the kth pixel in the ith cluster; $v_i (i = 1, 2, \cdots c)$in the clustering centre set $V = \{v_1, v_2 \cdots v_c\}$represents the ith clustering centre;$c$represents the cluster number; and $n$means the number of the total pixels in the image. The weighting exponent$m$ controls the fuzziness of the cluster; $x_k$means the grey of the kth pixel; and$\|x_k - v_i\|$represents the Euclidean distance between the kth pixel and the ith clustering centre. The objective function in Eq. (5) can be rewritten as follows using the Lagrange multiplier λ:

$$J_m^{'}(U,V) = \sum_{i=1}^{c}\sum_{k=1}^{n} u_{ik}^m \|x_k - v_i\|^2 + \lambda\left(\sum_{i=1}^{c} u_{ik} - 1\right) \quad (6)$$

Taking the first derivatives of $J_m^{'}(U,V)$with respect to $u_{ik}$and $v_i$and setting the results to zero, we can update the center$u_{ik}$and the membership v_i as follows.

$$v_i = \sum_{k=1}^{n} u_{ik}^m x_k \Big/ \sum_{k=1}^{n} u_{ik}^m, \;\; i = 1, 2, \cdots, c. \quad (7)$$

$$u_{ik} = \|x_k - v_i\|^{\frac{-2}{m-1}} \Big/ \sum_{j=1}^{c} \|x_k - v_j\|^{\frac{-2}{m-1}}, \; i = 1, 2, \cdots, c; \; k = 1, 2, \cdots, n. \quad (8)$$

As stated previously, defect segmentation in a noisy MPSG image is not reliable when using FCM. Based on the spatial constraint,

Table 2
Membership of u_{ik},$\bar{u}_{ir}$and $u_{ik}^{'}$in Fig. 5.

	u_{ik}	$\bar{u}_{ir}$	$u_{ik}^{'}$
(a)	0.8000	0.2875	0.6174
(b)	0.2000	0.7125	0.3826
(c)	0.4000	0.2875	0.2120
(d)	0.6000	0.7125	0.7880

Ahmed et al. proposed a modified objective function (FCM_S) to solve this problem [46,47]:

$$\begin{aligned} &min \, J_m(U,V) = \sum_{i=1}^{c}\sum_{k=1}^{n} u_{ik}^m \|x_k - v_i\|^2 + \frac{\alpha}{N_R}\sum_{i=1}^{c}\sum_{k=1}^{n} u_{ik}^m \Big(\sum_{x_r \in N_k} \|x_r - v_i\|^2\Big) \\ &s.t. \sum_{i=1}^{c} u_{ik} = 1, \; i \in [1,c], \; k \in [1,n], \; u_{ik} > 0 \end{aligned} \quad (9)$$

where $x_r$represents the grey of the pixels in the neighbourhood$N_k (N_k = l \times l)$of the pixel x_k;$N_R$represents the number of pixels inN_k; and $\frac{\alpha}{N_R}\sum_{i=1}^{c}\sum_{k=1}^{n} u_{ik}^m\big(\sum_{x_r \in N_k} \|x_r - v_i\|^2\big)$is a trade-off term from the local neighbourhood information. The parameterα is a constant that controls the effect of the neighbourhood. We can obtain the iteration formula of the membership u_{ik} and the cluster centrev_i (see Eqs. (10) and (11), respectively) by minimizing the objective function in Eq. (9) in a similar fashion to the standard FCM:

$$v_i = \sum_{k=1}^{n} u_{ik}^m \Big(x_k + \frac{\alpha}{N_R}\sum_{x_r \in N_k} x_r\Big) \Big/ (1+\alpha)\sum_{k=1}^{n} u_{ik}^m, \; i = 1, 2, \cdots, c. \quad (10)$$

$$u_{ik} = 1 \Big/ \sum_{j=1}^{c} \left(\frac{\|x_k - v_i\|^2 + \frac{\alpha}{N_R}\sum_{x_r \in N_R} \|x_r - v_i\|^2}{\|x_k - v_j\|^2 + \frac{\alpha}{N_R}\sum_{x_r \in N_R} \|x_r - v_j\|^2} \right)^{\frac{1}{m-1}} ; \; i = 1, 2, \cdots c; \; k = 1, 2, \cdots, n. \quad (11)$$

This modified FCM achieved better segmentation results than the FCM method [46]; however, there is still room for further improvement. The membership relationships of the local pixels are near its neighbourhood; thus, we can revise the membership using the local neighbourhood information (see Eq. (12)):

$$u_{ik}^{'} = u_{ik}^p \bar{u}_{ir}^q \Big/ \sum_{i=1}^{c} u_{ik}^p \bar{u}_{ir}^q \quad (12)$$

where $\bar{u}_{ir}$represents the average membership of the neighbouring pixels$x_r$in the ith cluster; $u_{ik}^{'}$is the revised membership of u_{ik}; and$p$and q are constant parameters that balance the effects of u_{ik} and $\bar{u}_{ir}$, respectively. This study aims to segment defects from the background of the MPSG image with$c = 2$.When$\bar{u}_{ir} > 0.5$, $u_{ik}^{'} > u_{ik}$.When$\bar{u}_{ir} < 0.5$,$u_{ik}^{'} < u_{ik}$. Four local neighbourhood membership features with a 3×3 window are shown in Fig. 5 where u_{ik}represents the membership of the central pixel in a 3×3 window, $\bar{u}_{ir}$is the average membership of the pixels in the neighbourhood, and$u_{ik}^{'}$is the revised value of u_{ik}used in Eq. (12).

The membership of the noise is distinctly different from its neighbouring pixels in Fig. 5 (a–b). Conversely, the membership of the homogenous pixel is near its neighbouring pixels in Fig. 5(c–d).The revised membership$u_{ik}^{'}$ of the noise and the homogenous pixels tend toward their own average$\bar{u}_{ir}$compared with their original membershipu_{ik}, as shown in Table 2.This indicates that they are considerably closer to the majority of their

0.2000	0.3000	0.4000
0.2000	0.8000	0.2000
0.3000	0.3000	0.4000

(a) the noise in the center with its $\overline{u}_{ir} < 0.5$

0.8000	0.7000	0.6000
0.8000	0.2000	0.8000
0.7000	0.7000	0.6000

(b) the noise in the center with its $\overline{u}_{ir} > 0.5$

0.2000	0.3000	0.4000
0.2000	0.4000	0.2000
0.3000	0.3000	0.4000

(c) the homogenous pixel in the center with its $\overline{u}_{ir} < 0.5$

0.8000	0.7000	0.6000
0.8000	0.6000	0.8000
0.7000	0.7000	0.6000

(d) the homogenous pixel in the center with its $\overline{u}_{ir} > 0.5$

Fig. 5. Local neighbourhood membership with a 3×3 window.

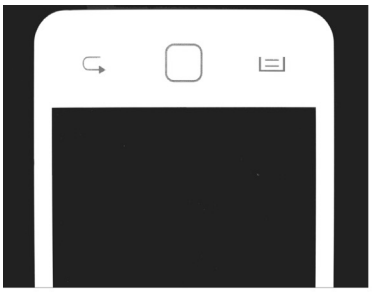

(a)The template

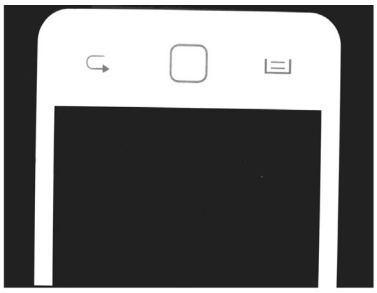

(b) The image with a small rotation and displacement

Fig. 6. Images to be aligned.

local neighbouring pixels. Noisy pixels are clustered based on the membership of their local neighbouring pixels, which significantly improves the segmentation results of a noisy image.

The acquired cluster centre using the fast FCM algorithm based on a histogram [48] is set to the initial centre to decrease the number of the iteration. The steps for defect segmentation in the MPSG image are described as follows.

Step1. Confirm the initial parameters. In this study,$c = 2$, $m = 2$, $p = q = 1$, $\alpha = 0.3$, $l = 3$ and $\varepsilon = 10^{-4}$.

Step2. Compute the initial cluster centresv_i using the fast FCM algorithm.

Step3. Compute the membership u_{ik} using Eq. (11), and obtain the revised membership u'_{ik} using Eq. (12) and the new cluster centresv_i using Eq. (10) by substituting $u'_{ik}$for u_{ik}.

Step4. Repeat step3 until the following termination creation is satisfied:

$$\|v_i^{t+1} - v_i^t\| \leq \varepsilon$$

The final segmentation result is then obtained.

4. Experimental verification

In this section, to evaluate the performance of the proposed methods and automatic defect detection system, we presented four experiments: (1) comparing the proposed contour-based registration (CR) with three other methods, (2) evaluating the performance of the proposed combination of subtraction and projection (CSP), (3) comparing the proposed IFCM with other versions of improved FCM and the common threshold segmentation methods, and (4) providing the testing speed results for the proposed automatic defect detection system. The methods in the experiments were implemented on an Intel Core i3-2100, 3.10 GHz personal computer in MATLAB. The test images were obtained through the experimental platform introduced in section 3.1 in the following experiment.

4.1. Performance of the proposed contour-based registration (CR)

The template was produced using the average of multiple non-defective images in this experiment (see Fig. 6 (a)). The image in Fig. 6 (b) can be obtained by rotating and displacing the template in Fig. 6 (a). Mutual information (MI) and the corner-based methods are common technologies in rigid registration. For comparison, the image in Fig. 6 (b) was aligned with the template in Fig. 6 (a) using the proposed CR method, the PSO-based MI method [49] the Powell-based MI method [50] and the Harris corner-based registration (HCBR) [51], and the results were shown in Table 3. We introduced the *individual error* (*IE*) to evaluate the registration accuracy as follows:

$$IE = |V_m - V_r| \tag{13}$$

where $V_m$means the measurement from the registration method and $V_r$means its real value.

Table 3 shows that the PSO-based MI method, the HCBR method and the proposed CR method achieved nearly equal sub-pixel accuracies, which were better than the Powell-based MI method. The Powell-based MI method completed more quickly compared to the PSO-based MI method; however, it was hard to locate the global minimum because this method tended to locate local minimums easily. Strictly speaking, the *IEs* of the PSO-based MI method and the HCBR method were lower than the proposed CR method; however, these improved *IEs* required 722.0813s and 6.7159s to complete its computations respectively, which were significantly more than the proposed CR method's computation time of 1.0917s; thus, the PSO-based MI method and the HCBR method cannot meet the needs of online detection. For a test image of size $m \times n$, the computational complexities of the Powell-based MI method, the PSO-based MI method, the HCBR method and the proposed CR method are $O(mni_1i_2)$, $O(pmni)$,$O(mn)$and $O(rn)$ respectively where i_1,$i_2$and $i$are the iteration numbers, $p$means population size, and $r$means the row of a small region containing touch keys. The computational

Table 3
Results of the alignment between Fig. 6 (b) and (a).

		Method							
		Powell-based MI [49]		PSO-based MI [50]		HCBR [51]		Proposed CR method	
	V_r	V_m	IE	V_m	IE	V_m	IE	V_m	IE
Δx (pixel)	3	1.1609	1.8391	3.0326	0.0326	3.0330	0.0330	2.9656	0.0344
Δy (pixel)	4	4.0381	0.0381	4.0077	0.0077	4.0040	0.0040	4.0134	0.0134
$\Delta\theta$(degree)	1	1.0047	0.0047	1.0009	0.0009	1.0011	0.0011	0.9979	0.0021
Time (s)		384.8699		722.0813		6.7159		1.0917	

Table 4
Average *IE* results of aligning 50 pairs of MPSG1 images.

	Methods			
	Powell-based MI [49]	PSO-based MI [50]	HCBR [51]	Proposed CR method
Δx (pixel)	0.9985	0.0279	0.0319	0.0287
Δy (pixel)	2.0104	0.0052	0.0066	0.0323
$\Delta\theta$(degree)	0.0024	0.0006	0.0009	0.0016
Runtime (s)	207.4811	770.1948	5.6264	1.2035

Table 5
Average *IE* results of aligning 50 pairs of MPSG2 images.

	Methods			
	Powell-based MI [49]	PSO-based MI [50]	HCBR[51]	Proposed CR method
Δx (pixel)	2.5351	0.0171	0.0342	0.0182
Δy (pixel)	0.4907	0.0741	0.0766	0.0914
$\Delta\theta$(degree)	0.0085	0.0013	0.0025	0.0024
Runtime (s)	212.3390	819.5091	5.8096	1.1735

Table 6
Confusion matrix.

		Detected	
		Positive	Negative
Actual	Positive	True Positive (TP)	False Negative (FN)
	Negative	False Positive (FP)	True Negative (TN)

complexities of the Powell-based MI method and the PSO-based MI method increase with rising iteration numbers or population size, therefore their complexities are far larger than that of the HCBR and the proposed CR method. Compared with the proposed CR method, the computation complexity of the HCBR method is still high. It is mainly caused by complex Gauss convolution computation and feature point response function computation in every pixel throughout the test image. Considering the small displacement and rotation in MPSG test image, the proposed CR method extracted the contours of touch keys only in a small region which probably contains touch keys. Since the row $r$in the small region is much less than the row m in the entire image, that is, $r < m$, the proposed CR method is faster than the HCBR method for alignment. We also tested the speed of the HCBR in such a small region of MPSG, and the time consuming was 1.6702s, slightly greater than that of the proposed CR method (1.0917s). The reason may be that the HCBR spends much time in removing unrelated corners and finding the corresponding corners.

We aligned 50 pairs of two different kinds of MPSG images (denoted as MPSG1 and MPSG2 respectively, see Fig. 7) to evaluate the robustness of the proposed CR method. Tables 4 and 5 show the average *IE* results and the runtime achieved by the various methods in this experiment, respectively. From Tables 4 and 5, we can see that the proposed CR method achieved fewer *IE* values than the Powell-based MI method and approximately equal *IE* values to the PSO-based MI method and the HCBR method. The proposed CR method took up a little more than 1 s on average to align a pair of images, which was considerably less than other methods. From the results of Tables 4 and 5, the proposed CR method was much better than the Powell-based MI and approximately equal to the PSO-based MI and the HCBR method in the accuracy. The proposed CR method was much faster than other methods used in the speed.

4.2. Performance of the proposed combination of subtraction and projection (CSP)

In this section, the test images contain 50 defective images and 150 non-defective images. These 200 images were obtained in different periods during the second six months of the year 2013. The test images are 2500×2000 pixels, 8-bit grey images (BMP format). The resolutions of the test images are approximately 0.0325 mm/pixel. Multiple non-defective images were aligned using the proposed contour-based registration, and the average values of multiple aligned images were considered as the template image for implementing the subtraction operation. In this experiment, we tested three methods: (1) image subtraction after the contour-based registration (IS), (2) direct image subtraction without the registration (DIS), and (3) the combination of image subtraction and greyscale projection after the contour-based registration (CSP). Here, we introduced the confusion matrix shown in Table 6. In Table 6, "positive" means defective images, and "negative" means non-defective images.

where TP means defective images that are correctly identified as defective. FP means non-defective images that are incorrectly identified as defective. TN means non-defective images that are correctly identified as non-defective. FN means defective images that are incorrectly identified as non-defective. The performance of the IS, DIS and CSP methods can be evaluated by using two indices called sensitivity and specificity, defined by

$$sensitivity = \frac{\#TP}{\#TP + \#FN} \times 100\% \quad (14)$$

$$specificity = \frac{\#TN}{\#TN + \#FP} \times 100\% \quad (15)$$

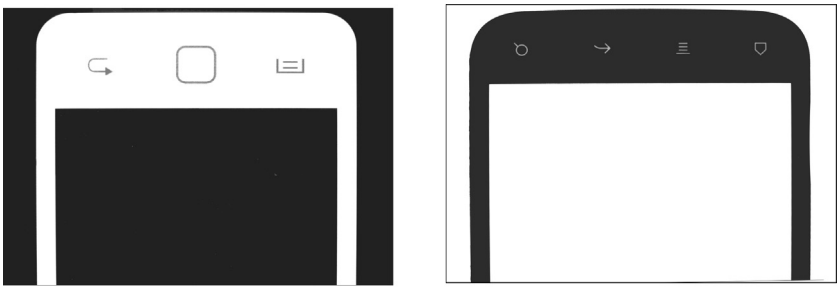

MPSG1 (b) MPSG2

Fig. 7. Two different kinds of MPSG images for alignment.

Table 7
Experimental results of the confusion matrix using different methods.

		IS		DIS		CSP	
		Detected		Detected		Detected	
		Defective	Non-defective	Defective	Non-defective	Defective	Non-defective
Actual	Defective	45	5	40	10	47	3
	Non-defective	9	141	13	137	4	146

Table 8
Sensitivity and specificity results using different methods.

	IS	DIS	CSP
sensitivity	90%	80%	94%
specificity	94%	91.33%	97.33%

Table 9
UR of segmented defects using different methods.

Method	Otsu [52]	Niblack [53]	Kittler [54]	Proposed IFCM
UR	0.9158	0.9095	0.8754	0.9371

where # means the "number of ". Sensitivity means a ratio in which the defective images are identified as the defective images by the method, and specificity means a ratio in which the non-defective images are identified as the non-defective images. A good method should achieve a high sensitivity and specificity.

In this experiment, Table 7 shows the results of the confusion matrix achieved by three methods, and the results of the sensitivity and the specificity are shown in Table 8. From Table 8, we can see that the CSP method achieves 94% in sensitivity and 97.33% in specificity, superior to the IS and DIS methods. Specifically, three defective images are incorrectly identified as non-defective images, and four non-defective images are incorrectly identified as defective images when using the CSP method. There are two problems to consider when detecting the surface defects of an MPSG. One problem is the misalignment of the test image caused by the experimental platform vibration. The other problem is the grey fluctuation of the test image caused by the surrounding illumination changes during the six months of capturing test images. The IS method does not consider the second problem, and the DIS method does not consider either of the two problems. The CSP method considers the impact of these two problems on the test images and implements the CR method and the CSP method to solve the two problems, respectively. Therefore, the CSP method outperforms the IS method and the DIS method in terms of sensitivity and specificity.

4.3. Performance of fuzzy boundary defect segmentation using the proposed IFCM method

The residual image can be obtained through the subtraction of the test image and the template image. The presence/absence of a defect can be determined in the residual image using the proposed CSP method. The defects, if they exist, can be segmented using the proposed IFCM method in the residual image in this section. The size of the defect is very small in the test image, see Fig. 8(a); therefore, to compare the segmentation performance visually, a region with a defect (see Fig. 8(b)) is extracted and resized to a 23×21 matrix from the residual image in the experiments. In Fig. 8 (b), there is a fuzzy grey boundary and a small grey difference between the defect (the darker area) and the background (the lighter area). The 23 × 21 pixel region with the defect is used for the following defect segmentation experiment.

4.3.1. Segmentation comparison with the common threshold segmentation methods

The threshold method is a common technology used to segment objects from an image background; however, a suitable threshold must be set. In this study, three common threshold methods are investigated (*i.e.*, those of Otsu [52], Niblack [53] and Kittler [54]); the segmentation performance of these methods with an MPSG image is then compared with the proposed IFCM method. The segmentation results are shown in Fig. 9. The uniformity of the intra region (UR), which is defined as follows, is used to evaluate the defect segmentation performance [55].

$$UR = 1 - \frac{1}{N}\sum_{i=1}^{c}\frac{\sum_{x_k \in R_i}\left(x_k - \frac{1}{N_{R_i}}\sum_{x_k \in R_i} x_k\right)^2}{\left(\max_{x_k \in R_i} x_k - \min_{x_k \in R_i} x_k\right)^2} \tag{16}$$

where the image is segmented into $c$portions. In this study, $c = 2$ and represents defects and free of defects; $N$is the total number of pixels in the image;R_i is the ith partition; $x_k$is the grey value of the kth pixel in R_i; and$N_{R_i}$is the total number of pixels in R_i. The results of the UR are listed in Table 9.

From Fig. 9, the defects found using the proposed IFCM method are located more closely compared to the threshold techniques; the proposed IFCM method also achieves better boundary segmentation. It is shown in Table 9 that the UR from the proposed IFCM method performs better than those of the other methods. This finding indicates that there is a best grey uniformity of the segmented

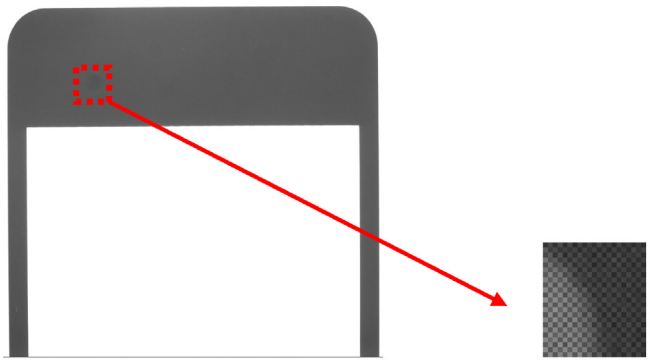

(a) A defective test image (b) A small region containing a defect

Fig. 8. A defective test image and a small region with a defect.

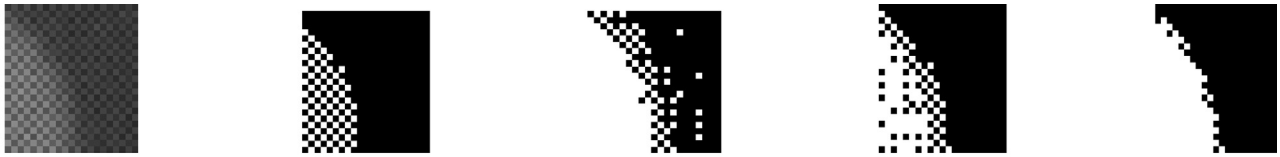

(a) original image (b) Kittler (c) Niblack (d) Otsu (e) IFCM

Fig. 9. Segmentation results using different methods.

defect region when using the proposed IFCM method compared to the three threshold methods.

4.3.2. Segmentation comparison with other versions of improved FCM

The FCM_S method uses all of the neighbouring pixels of each pixel during the iterations and is very time consuming to complete. To reduce the computational complexity of the FCM_S method, Chen and Zhang [56] proposed two variant versions based on the FCM_S method: FCM_S1 and FCM_S2. The neighbourhood average operation in FCM_S1 and the neighbourhood median operation in FCM_S2 replace the neighbouring pixel operation in FCM_S. Wang proposed a modified membership function for the FCM method (*i.e.*, the FCM_M method) to improve the performance in the presence of noise [57]. In this section, the segmentation results from the MPSG image using the FCM, FCM_S, FCM_S1, FCM_S2, and FCM_M methods and the proposed IFCM algorithm are shown in Fig. 10. In the experiment, $\alpha = 0.3$ and$N_R = 3 \times 3$.We use three cluster validity indices of the Xie-Beni criterion (V_{XB}) [58], the partition coefficient (V_{pc}) [59] and the partition entropy (V_{pe}) [60], which are defined as follows, to evaluate the methods' robustness to the noise. When the pixels are clustered optimally, a smaller V_{XB} and V_{pe} and a larger $V_{pc}$are obtained:

$$V_{XB} = \frac{\sum_{i=1}^{c}\sum_{j=1}^{n} u_{ij}^2 \|x_j - v_i\|^2}{n \min_{i \neq j} \|v_i - v_j\|} \tag{17}$$

$$V_{pc} = \frac{\sum_{i=1}^{c}\sum_{j=1}^{n} u_{ij}^2}{n} \tag{18}$$

Table 10
Validity of the cluster indices for defect segmentation.

Method	V_{XB}	V_{pe}	V_{pc}
FCM [61]	0.0914	0.2811	0.8206
FCM_S [46,47]	0.0719	0.2744	0.8413
FCM_S1 [56]	0.0709	0.2369	0.8643
FCM_S2 [56]	0.0652	0.2522	0.8527
FCM_M [57]	0.0664	0.1260	0.9242
Proposed IFCM	0.0547	0.1071	0.9396

$$V_{pe} = -\frac{\sum_{i=1}^{c}\sum_{j=1}^{n} u_{ij} \log_b(u_{ij})}{n} \tag{19}$$

The results of the segmentations are shown in Fig. 10, and the validity of the cluster indices is presented in Table 10.

In Fig. 10, the cluster effect using the proposed IFCM method is superior to the other FCM methods because the defect pixels are located more closely even in the presence of noise, and the cluster effect using the FCM method performs very poorly because the noise in the background is incorrectly identified as defect pixels. From Table 10, it is shown that $V_{pc}$is the largest, andV_{pe} and V_{XB} are the smallest in the proposed IFCM method compared to the FCM method and its improved versions. This finding indicates that the proposed IFCM method performs best compared to the FCM method and the other improved FCM methods when segmenting a real MPSG image.

4.4. Speed performance of the proposed automatic defect detection system

The proposed automatic defect detection system consists of three stages: registration using the CR method (stage 1), defect detection using the CSP method (stage 2) and defect segmentation using the proposed IFCM method (stage 3). We test the average speed performance of the proposed defect detection system with

Fig. 10. Segmentation results of an MPSG image using different FCMs.

Table 11
AR of each stage and the proposed automatic defect detection system (s).

	Stage 1	Stage 2	Stage 3	Total
AR	1.1079	0.0354	0.5168	1.6601

100 test images from the input to the final output. We present the average runtime (AR) of each stage and the overall automatic defect detection system in Table 11. From Table 11, we can see that stage 1 takes up 1.1079s, accounting for 66.74% (1.1079/1.6601 × 100%) of the total AR (1.6601s). Considerable time is spent searching for the pairwise contours in stage 1. Stage 2 is responsible for 2.11% (0.0354/1.6601 × 100%) of the total AR. Stage 2 is the fastest stage among the three stages because this is the only stage involved in the pixel algorithm operation. Based on stage 1 and stage 2, we can determine whether a test MPSG has the defect; therefore, these two stages should work for high speed. The AR sum of stage 1 and stage 2 in this experiment is 1.1433s (1.1079s + 0.0354s, 68.87% of the total AR), which can meet the needs of online detection. The AR of stage 3 is 0.5168s (31.13% of the total AR), and stage 3 only works for the defective test MPSG, which has fewer real-time requirements than stage 1 and stage 2.

5. Conclusions

The process of manufacturing a mobile phone screen will unavoidably cause various surface defects that are currently inspected primarily by human eyes. In this study, a vision-based defect detection system is proposed to automatically inspect mobile phone screens in a mobile phone production line. A contour-based image registration algorithm is used to resolve any misalignments in the acquired images due to their rotation and displacement caused by stage vibration. Using image subtraction and greyscale projection, the defects on a screen can be identified; the method used will not be affected by fluctuation in the surrounding illumination. To solve the problem of segmenting defects with fuzzy grey boundaries from a noisy MPSG image, an improved fuzzy c-means cluster (IFCM) algorithm is proposed and validated in this study. The detection system for the MPSG was implemented in MATLAB. Several experimental tests have been performed, and the results show that the method proposed in this study can achieve a satisfying detection result and that it has better performance compared to previous methods. Based on this study, the classification of detected defects will be considered in a future study to aid in repair decision-making.

Acknowledgments

This work was supported in part by the National Natural Science Foundation of China (Grant no. 51275093, no. 51675106), Guangdong Provincial Natural Science Foundation (Grant no. 2015A030312008), and in part by the Guangdong Provincial R&D Key Projects (Grant no. 2015B010104008, no. 2016A030308016).

References

[1] J. Atzlesberger, B.G. Zagar, R. Cihal, M. Brummayer, P. Reisinger, Sub-surface defect detection in a steel sheet, Meas. Sci. Technol. 24 (2013).
[2] Q. Li, S. Ren, A visual detection system for rail surface defects, IEEE Trans. Syst. Man Cybern. Part C-Appl. Rev. 42 (2012) 1531–1542.
[3] Y.-H. Liu, S.-H. Lin, Y.-L. Hsueh, M.-J. Lee, Automatic target defect identification for TFT-LCD array process inspection using kernel FCM-based fuzzy SVDD ensemble, Expert Syst. Appl. 36 (2009) 1978–1998.
[4] Y. Ma, X. Sun, G. Li, X. Wang, Ieee surface defect detection based on capacitive probe for bearing ball, 2013 25th Chinese Control and Decision Conference (2013) 2037–2040.
[5] L.-Q. Liang, D. Li, X. Fu, W.-J. Zhang, Touch screen defect inspection based on sparse representation in low resolution images, Multimedia Tools Appl. 75 (2016) 2655–2666.
[6] D. Li, L.-Q. Liang, W.-J. Zhang, Defect inspection and extraction of the mobile phone cover glass based on the principal components analysis, Int. J. Adv. Manuf. Technol. 73 (2014) 1605–1614.
[7] J. Torng, K.K. Maung, K.-C. Fan, Development of an automated optical inspection system for mobile phone panels, Journal of the Chinese Society of Mechanical Engineers Transactions of the Chinese Institute of Engineers, Series C/Chung-Kuo Chi Hsueh Kung Ch'eng Hsuebo Pao 34 (2013) 103–108.
[8] V. Kecman, Learning and Soft Computing: Support Vector Machines, Neural Networks, and Fuzzy Logic Models, MIT press, 2001.
[9] L. Wang, X. Fu, Data Mining with Computational Intelligence, Springer Science & Business Media, 2006.
[10] V. Mitra, C.-J. Wang, S. Banerjee, Lidar detection of underwater objects using a neuro-SVM-based architecture, IEEE Trans. Neural Netw. 17 (2006) 717–731.
[11] Y.H. Liu, Y.K. Huang, M.J. Lee, Automatic inline defect detection for a thin film transistor?liquid crystal display array process using locally linear embedding and support vector data description, Meas. Sci. Technol. 19 (2008) 095501.
[12] X. Zhang, C. Gu, J. Lin, Support vector machines for anomaly detection, Intelligent Control and Automation, 2006. WCICA 2006. The Sixth World Congress On, IEEE (2006) 2594–2598.
[13] T. Du-Ming, K. Chih-Chia, Defect detection in inhomogeneously textured sputtered surfaces using 3D Fourier image reconstruction, Mach. Vision Appl. 18 (2007) 383–400.
[14] J. Chang-Do, K. Se-Yun, L. Hee-Yul, Y. Byoung-Ju, L. Joon-Jae, L. Young-Do, P. Kil-Houm, Fourier Spectrum based Periodic Cell Pattern Elimination in Thin Film Transistor Liquid Crystal Display Cell Image, in: 2011 IEEE International Conference on Consumer Electronics (ICCE), 9–12 Jan. 2011, IEEE Piscataway, NJ, USA, 2011, pp. 871–872.
[15] L. Chi-Jie, T. Du-Ming, Automatic defect inspection for LCDs using singular value decomposition, Int. J. Adv. Manuf. Technol. 25 (2005) 53–61.
[16] J.-L. Bouchot, G. Stübl, B. Moser, A template matching approach based on the discrepancy norm for defect detection on regularly textured surfaces.
[17] J. Jing, S. Chen, P. Li, Automatic defect detection of patterned fabric via combining the optimal gabor filter and golden image subtraction, J. Fiber Bioeng. Inf. 8 (2015) 229–239.
[18] J. Kim, Template-based defect detection of a brazed heat exchanger using an x-ray image, Opt. Eng. 52 (2013), 036501–036501.
[19] P. Xie, S.-U. Guan, A golden-template self-generating method for patterned wafer inspection, Mach. Vision. Appl. 12 (2000) 149–156.
[20] P.B. Chou, A.R. Rao, M.C. Sturzenbecker, F.Y. Wu, V.H. Brecher, Automatic defect classification for semiconductor manufacturing, Mach. Vision. Appl. 9 (1997) 201–214.
[21] X. Bai, Y. Fang, W. Lin, L. Wang, B.-F. Ju, Saliency-based defect detection in industrial images by using phase spectrum, IEEE Trans. Ind. Inf. 10 (2014) 2135–2145.
[22] D.-M. Tsai, C.-P. Lin, Fast defect detection in textured surfaces using 1D Gabor filters, Int. J. Adv. Manuf. Technol. 20 (2002) 664–675.
[23] M.L. Raymer, W.F. Punch, E.D. Goodman, L.A. Kuhn, A.K. Jain, Dimensionality reduction using genetic algorithms, IEEE Trans. Evol. Comput. 4 (2000) 164–171.
[24] X. Fu, L. Wang, Data dimensionality reduction with application to simplifying RBF network structure and improving classification performance, IEEE Trans. Syst. Man Cybern. Part B: Cybern. 33 (2003) 399–409.
[25] F. Ratle, G. Camps-Valls, J. Weston, Semisupervised neural networks for efficient hyperspectral image classification, IEEE Trans. Geosci. Remote Sens. 48 (2010) 2271–2282.
[26] G. Giacinto, F. Roli, Design of effective neural network ensembles for image classification purposes, Image Vision Comput. 19 (2001) 699–707.

[27] G. Stübl, J.-L. Bouchot, P. Haslinger, B. Moser, Discrepancy Norm as Fitness Function for Defect Detection on Regularly Textured Surfaces, Springer, 2012.
[28] G. Stübl, B. Moser, J. Scharinger, On approximate nearest neighbour field algorithms in template matching for surface quality inspection, in: Computer Aided Systems Theory-EUROCAST, Springer, 2013, 2013, pp. 79–86.
[29] X.H. Hou, H.H. Liu, Research of background modeling algorithm method based on multi-frame average method in moving target detection, in: 2013 International Conference on Vehicle and Mechanical Engineering and Information Technology, VMEIT 2013, August 17, 2013–August 18, 2013, Trans Tech Publications Ltd, Zhengzhou, Henan, China, 2013, pp. 1390–1393.
[30] W. Zhiliang, G. Jian, C. Xin, Z. Weiming, Organic light emitting diode pixel defect detection through patterned background removal, Sens. Lett. 11 (2013) 356–361.
[31] J. Chen, An improved registration method using the criterion of five-coplanar points, Optik—Int. J. Light Electron Optics 127 (2016) 390–395.
[32] G. Wang, Z. Wang, Y. Chen, W. Zhao, Robust point matching method for multimodal retinal image registration, Biomed. Signal Process. Control 19 (2015) 68–76.
[33] B. Zitová, J. Flusser, Image registration methods: a survey, Image Vision Comput. 21 (2003) 977–1000.
[34] L. Wang, N.H.C. Yung, Extraction of moving objects from their background based on multiple adaptive thresholds and boundary evaluation, IEEE Trans. Intell. Transp. Syst. 11 (2010) 40–51.
[35] S. Liao, G., Zhao, V., Kellokumpu, M. Pietik, x00E, inen, S.Z., Li, Modeling pixel process with scale invariant local patterns for background subtraction in complex scenes, in: Computer Vision and Pattern Recognition (CVPR), 2010 IEEE Conference on, 2010, pp. 1301–1306.
[36] H.H. Lin, J.H. Chuang, T.L. Liu, Regularized background adaptation: a novel learning rate control scheme for gaussian mixture modeling, IEEE Trans. Image Process. 20 (2011) 822–836.
[37] D.-S. Lee, Effective gaussian mixture learning for video background subtraction, IEEE Trans. Pattern Anal. Mach. Intell. 27 (2005) 827–832.
[38] H. Wang, D.-s. Zhu, W. Tang, An algorithm of strip surface defect detection based on grayscale projection, Northeast. Univ. (Natural Science) 29 (2008) 375–377.
[39] A. Hashioka, K. Kuramoto, S. Kobashi, Y. Wakata, K. Ando, R. Ishikura, T. Ishikawa, S. Hirota, Y. Hata, Fuzzy object shape model for newborn brain MR image segmentation, Soft Computing and Intelligent Systems (SCIS) and 13th International Symposium on Advanced Intelligent Systems (ISIS), 2012 Joint 6th International Conference on (2012) 1253–1258.
[40] X. Bi, C. Zhuang, H. Ding, A new mura defect inspection way for TFT-LCD using level set method, IEEE Signal Process Lett. 16 (2009) 311–314.
[41] R. He, Y. Zhu, A Hybrid Image Segmentation Approach Based on Mean Shift and Fuzzy C-Means, (2009), 105–108.
[42] Y. Qiuxia, T. Liangrui, Q. Bing, Z. Jing, A New FCM-Based Algorithm of Hydrophobic Image Segmentation, 2009, 374–377.
[43] R.R.d. Vargas, B.R.C., Bedregal, E.S. Palmeira, A Comparison between K-Means, FCM and ckMeans Algorithms, (2011) 32–38.
[44] Q. Chen, E. Petriu, X. Yang, A comparative study of fourier descriptors and Hu's seven moment invariants for image recognition, in: Canadian Conference on Electrical and Computer Engineering; Technology Driving Innovation, 2004, May 2, 2004–May 5, 2004, Institute of Electrical and Electronics Engineers Inc., Niagara Falls, Canada, 2004, pp. 0103–0106.
[45] J.C. Dunn, A fuzzy relative of the ISODATA process and its use in detecting compact well-separated clusters, J. Cybern. 3 (1974) 32–57.
[46] M.N. Ahmed, S.M. Yamany, N. Mohamed, A.A. Farag, T. Moriarty, A modified fuzzy C-means algorithm for bias field estimation and segmentation of MRI data, IEEE Trans. Med. Imaging 21 (2002) 193–199.
[47] M.N. Ahmed, S.M. Yamany, A.A. Farag, T. Moriarty, Bias field estimation and adaptive segmentation of MRI data using a modified fuzzy C-means algorithm, in: Proceedings. 1999 IEEE Computer Society Conference on Computer Vision and Pattern Recognition, 23–25 June 1999, IEEE Comput. Soc, Los Alamitos, CA, USA, 1999, pp. 250–255.
[48] L. Szilagyi, Z. Benyo, S.M. Szilagyi, H.S. Adam, MR brain image segmentation using an enhanced fuzzy C-Means algorithm, in: A New Beginning for Human Health: Proceedings of the 25th Annual International Conference of the IEEE Engineering in Medicine and Biology Society, September 17, 2003–September 21, 2003, Institute of Electrical and Electronics Engineers Inc., Cancun, Mexico, 2003, pp. 724–726.
[49] L. Qi, J. Hongbing, Medical image registration based on maximization of mutual information and particle swarm optimization, in: Fifth International Conference on Photonics and Imaging in Biology and Medicine, 1–3 Sept. 2006, SPIE ? The International Society for Optical Engineering, USA, 2007, pp. 65341–65342.
[50] J. Xu, J. Li, Y. Wang, H. Liang, D. Tian, N. Zhang, Z. Wang, W. Cong, Image registration based on MI and PSO algorithm, in: 2011 International Conference on Materials Engineering for Advanced Technologies, ICMEAT 2011, May 5, 2011–May 6, 2011, Trans Tech Publications Singapore, Singapore, 2011, pp. 569–573.
[51] Y. Pei, H. Wu, J. Yu, G. Cai, Effective image registration based on improved Harris corner detection, in: 2010 International Conference on Information, Networking and Automation, ICINA 2010, October 17, 2010–October 19, 2010, IEEE Computer Society, Kunming, China, 2010, pp. V193–V196.
[52] N. Otsu, Threshold selection method from gray-level histograms, IEEE Trans. Syst. Man Cybern. SMC-9 (1979) 62–66.
[53] S. Farid, F. Ahmed, Application of Niblack's method on images, in: 2009 International Conference on Emerging Technologies, ICET 2009, October 19, 2009–October 20, 2009, IEEE Computer Society, Islamabad, Pakistan, 2009, pp. 80–286.
[54] X. Jing-Hao, Z. Yu-Jin, Ridler and Calvard's, Kittler and Illingworth's and Otsu's methods for image thresholding, Pattern Recognit. Lett. 33 (2012) 793–797.
[55] P.K. Sahoo, S. Soltani, A.K.C. Wong, Y.C. Chen, A survey of thresholding techniques, Comput. Vision Graphics Image Process. 41 (1988) 233–260.
[56] C. Songcan, Z. Daoqiang, Robust image segmentation using FCM with spatial constraints based on new kernel-induced distance measure, IEEE Trans. Syst. Man Cybern. Part B (Cybernetics) 34 (2004) 1907–1916.
[57] P. Wang, H. Wang, A Modified FCM Algorithm for MRI Brain Image Segmentation, 2008, 26–29.
[58] X.L. Xie, G. Beni, A validity measure for fuzzy clustering, IEEE Trans. Pattern Anal. Mach. Intell. 13 (1991) 841–847.
[59] J.C. Bezdek, Cluster validity with fuzzy sets, J. Cybern. 3 (1973) 58–73.
[60] J.C. Bezdek, Mathematical Models for Systematics and Taxonomy, 1975.
[61] J.C. Bezdek, L.O. Hall, L.P. Clarke, Review of MR image segmentation techniques using pattern recognition, Med. Phys. 20 (1993) 1033–1048.